Applied Catalysis B: Environmental 224 (2018) 276–282

Contents lists available at ScienceDirect

Applied Catalysis B: Environmental

journal homepage: www.elsevier.com/locate/apcatb

Research paper

Egg-shell membrane reactors for nitrite hydrogenation: Manipulating kinetics and selectivity

Roger Brunet Espinosa[a,1], Damon Rafieian[b], Rolf Sybren Postma[a], Rob G.H. Lammertink[b], Leon Lefferts[a,*]

[a] Catalytic Processes and Materials Group, Faculty of Science and Technology, MESA + Institute for Nanotechnology, University of Twente, PO Box 217, 7500 AE Enschede, The Netherlands, The Netherlands

[b] Soft matter, Fluidics and Interfaces Group, Faculty of Science and Technology, MESA + Institute for Nanotechnology, University of Twente, PO Box 217, 7500 AE Enschede, The Netherlands

ARTICLE INFO

Keywords:
Nitrite hydrogenation
Egg-shell
Membrane reactor
Carbon nano-fiber
Ammonia selectivity

ABSTRACT

A method to fabricate catalytic membrane contactor reactors with a Pd-egg-shell distribution has been developed on α-alumina tubes, allowing excellent control over the distribution of the active phase through the wall of the alumina tube. The performance of these catalytic membrane reactors has been assessed for nitrite hydrogenation. We have shown that manipulation of the thickness of the zone containing active phase induces different diffusion lengths for nitrite and hydrogen, strongly influencing activity and selectivity. Thick active layers have proved to be more selective to nitrogen, the desired product for purification of drinking water. Surprisingly, a thick layer with active phase also induced a negative apparent order in hydrogen, which is tentatively assigned to the fact that the ratio of concentrations of reactants, hydrogen and nitrite, varies extremely in the active zone.

1. Introduction

Catalysts in contact with reactants and/or products in both gas- and liquid-phase are highly relevant for the chemical industry [1–4]. Conventional multiphase reactors comprise slurry reactors operating with catalyst particles of typically tens of microns, *i.e.* stirred tanks or bubble columns, as well as packed bed trickle-phase reactors [4–8] with catalyst particles of a few mm typically. The most common problems encountered with slurry catalysts concerns the filtration section which is expensive and not very robust, since *e.g.* attrition of the catalyst particles creates fines that are difficult to separate from the liquid [4]. Catalytic packed bed trickle-phase reactors usually suffer from internal mass transfer limitations due to the relatively large catalyst support particles, necessary to limit the pressure drop. Additionally, the random packing of the catalyst bodies easily results in flow mal-distribution including stagnant zones and by-passes [4,5,9]. Structured catalytic reactors based on e.g. monoliths [10,11], foams [12–15], and cloth [16,17] have attracted special attention in the last decades since these circumvent the necessity of filtration combined with short diffusion lengths, similar to slurry catalysts.

Catalytic membrane reactors are an interesting alternative for multiphase reactions. One of their main advantages is the well-defined gas-liquid interface independent of the flow rates of both phases [6,18–23]. Several reviews have been published describing and classifying catalytic membrane reactors. The most commonly used classification is based on the role of the membrane and is divided in three categories, namely extractor, contactor and distributor [21,24,25]. Extractors are used to suppress consecutive reactions or to increase conversion of equilibrium-restricted conversions, by selectively extracting one of the products through the membrane, integrating catalytic conversion with separation. Contactors promote a good contact between the catalyst and the reactant *via* the use of catalytically active membranes, integrating catalytic conversion and mixing. Contactors are a specific version of distributors, enabling well controlled distribution of one of the reactants to the reaction zone, avoiding variations in concentration in the axial direction of the reactor. This type of operation is relevant in cases that the selectivity is strongly influenced by the concentration of one of the reactants, *e.g.* in nitrite hydrogenation [26] and selective oxidation reactions operating with low oxygen concentration because of safety concern [21].

The major disadvantage of catalytic membrane reactors in three-phase operation is poor mixing in the liquid phase, caused by the

* Corresponding author.
E-mail addresses: r.brunetespinosa@utwente.nl, roger.brunet@eurekite.co (R. Brunet Espinosa), d.rafieianboroujeni@utwente.nl (D. Rafieian), r.s.postma@utwente.nl (R.S. Postma), r.g.h.lammertink@utwente.nl (R.G.H. Lammertink), l.lefferts@utwente.nl (L. Lefferts).
[1] Present address: Eurekite, Enschede, The Netherlands.

http://dx.doi.org/10.1016/j.apcatb.2017.10.058
Received 26 October 2016; Received in revised form 19 October 2017; Accepted 26 October 2017
Available online 27 October 2017

laminar regimes of the liquid stream in the relatively narrow channel. Recent work carried by Pashkova et al. [27] and Vospernik et al. [28] showed how to improve mixing and transport in the liquid channel by introducing glass beads or a static mixer inside the membrane tube. A different approach to minimize transport limitations in the liquid reactants is miniaturizing the membrane reactor, thus decreasing the diffusion length [1,29].

Nitrate is a common inorganic contaminant that can be found even in drinking water. In the human body, it can easily convert to nitrite, endangering health *via* methemoglobinemia (blue baby syndrome) or *via* formation of some carcinogenic nitrosamines [4,30,31]. Catalytic hydrogenation is a very promising technique to eliminate nitrate and nitrite from drinking water since it can convert these inorganic contaminants into harmless nitrogen. However, avoiding the formation of the undesired by-product ammonia still presents a challenge. It is known that the selectivity of nitrite hydrogenation is strongly influenced by the H/N of reaction intermediates on the catalyst surface [32–36]. Therefore the selectivity of the nitrite hydrogenation can be manipulated via the local concertations of hydrogen and nitrite at the active sites, which depend on the transport rate of both hydrogen and nitrite. Thus, nitrite hydrogenation is a suitable model reaction to study the mass-transfer performance of catalytic membrane reactors.

In previous work we have shown that the selectivity to N_2 of the reaction benefits from the use of a membrane contactor reactor, based on Pd supported on CNFs inside the macro-pores of an α-alumina membrane, as compared to different reactor configurations co-feeding hydrogen and nitrite to the reaction zone [37]. In short, the membrane reactor allows decreasing the H/N ratio in the reaction zone via hydrogen dosing through the membrane, resulting in higher nitrogen selectivity, without compromising the conversion level. The catalytic membrane contactor reactors used so far contained CNFs and palladium distributed throughout the α-alumina tube. Here, we report on the effect of the distribution of palladium and CNFs inside the wall of the alumina tube, investigating the influence on conversion and selectivity. Differences are to be expected because of variation of the diffusion lengths to the active sites for both reactants, similar but not identical to egg-shell structures in conventional catalyst particles, as will be discussed in detail.

2. Experimental

2.1. Materials used

Porous ceramic alumina (α-Al_2O_3) hollow fibers with a length of 200 mm and an inner and outer diameter of 0.9 and 1.9 mm respectively, were purchased from Hyflux CEPAration Technologies, Europe. They were cut in pieces of 55 mm long to be used as catalyst support and as the skeleton of the reactor. Nickel nitrate hexahydrate (Merck), urea (Merck) and nitric acid (65%, Merck) were used to deposit nickel on the alumina hollow fibers. Ethylene (99.95% PRAXAIR), hydrogen and nitrogen (99.999% INDUGAS) were used to grow CNFs without any further purification. Palladium acetylacetonate (Alfa Aesar) and toluene (> 99.9%, Merck) were used to deposited palladium. Toluene (> 99.9% Merck) and a two component PDMS RTV 615 kit (permacol B.V.) consisting of a vinyl terminated pre-polymer (RTV-A) and a Pt-catalysed cross-linker (RTV-B) were used for the preparation of the PDMS solution. Sodium nitrite (> 99%, Merck) was used as nitrite source for the catalytic tests.

2.2. Fabrication of the reactors

The membrane reactors were synthesized as described elsewhere (submitted to Catalysis Today). In short, a hollow α-alumina fiber was loaded with small nickel particles using nickel deposition-precipitation technique. Afterwards, CNFs were grown using a quartz tube reactor of 10 mm diameter. The hollow alumina fiber was placed inside the quartz tube and the temperature was raised to 850 °C at 6 °C/min using 100 ml/min of nitrogen gas. After 1 h at 850 °C, a hydrogen/nitrogen mixture (50/50) was fed to the system for 2 h. Next, the temperature was cooled to 600 °C under 80 ml/min of nitrogen gas. The CNF growth was performed at 600 °C under a gas mixture containing 20% ethylene (C_2H_4), 7% H_2, and 73% N_2. Three different CNF growth times were studied: 15, 22.5 and 45 min. Next, the temperature was cooled to room temperature under 80 ml/min of nitrogen gas. Any loose CNFs were removed via sonication with miliQ water. After drying the sample, palladium was deposited on the CNFs using palladium acetylacetonate precursor and was then calcined and reduced at 250 °C. In the final step, the outer wall of the alumina fiber was coated with a home-made PDMS membrane. One of the reactors with CNFs grown for 45 min and without PDMS coating was crushed and sieved to a particle size of 125–250 μm.

2.3. Catalytic test

The synthesized membrane reactors were tested using the nitrite hydrogenation reaction under identical conditions. A nitrite solution (44 μmol/L NO_2^-) saturated with argon was introduced inside the tube with a flowrate of 0.05 ml/min, while the shell of the membrane reactor was exposed to a gas mixture containing between 0.02 and 1.0 bar of hydrogen, balanced with argon. In this configuration, hydrogen is allowed to diffuse to the reaction zone through the PDMS membrane located at the outer wall of the reactor. Hydrogen and nitrite meet and react at the palladium particles located at the CNFs.

The crushed reactor without PDMS was tested in a packed bed reactor. A nitrite solution (217 μmol/L NO_2^-) was pre-saturated in different hydrogen partial pressures (0.2, 0.5 and 1.0 bar) and fed to the catalytic bed.

All the tests were conducted at room temperature (20 °C). Nitrite and ammonium (NH_4^+) concentrations were measured at the inlet and outlet of the reactor with an in-line Ion Chromatograph (Dionex, ICS 1000). These values allowed calculating nitrite conversion and ammonia selectivity according to equations 1 and 2 respectively. The solutions were not buffered. Selectivity to nitrogen was calculated based on the mass balance and the fact that exclusively ammonia and nitrogen are formed under these conditions [32,35,38] (Fig. 1).

$$NO_2^- \text{conversion} = \frac{[NO_2^-]_{initial} - [NO_2^-]_{final}}{[NO_2^-]_{initial}} \cdot 100 \quad (1)$$

$$NH_4^+ selectivity = \frac{[NH_4^+]_{final} - [NH_4^+]_{final}}{[NO_2^-]_{initial} - NO_2^-]_{final}} \cdot 100 \quad (2)$$

2.4. Characterization

The BET surface areas of the membrane reactors were determined with N_2-adsorption obtained at 77 K (Micromeritics Tristar) using the BET isotherm. The location and morphology of the CNFs inside the pores in the wall of the membrane reactor as well as the palladium particle size were determined with High Resolution Scanning Electron Microscopy, HR-SEM (Analysis Zeiss MERLIN HR-SEM) equipped with EDX (Aztec, Oxford Instruments). Palladium particle size was determined by averaging 150 measurements on three different positions in the sample. Cross-sections were prepared with the help of a scalpel.

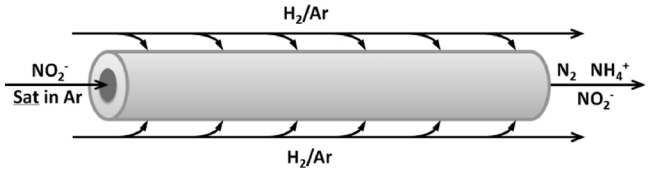

Fig. 1. Flow operation of a membrane reactor.

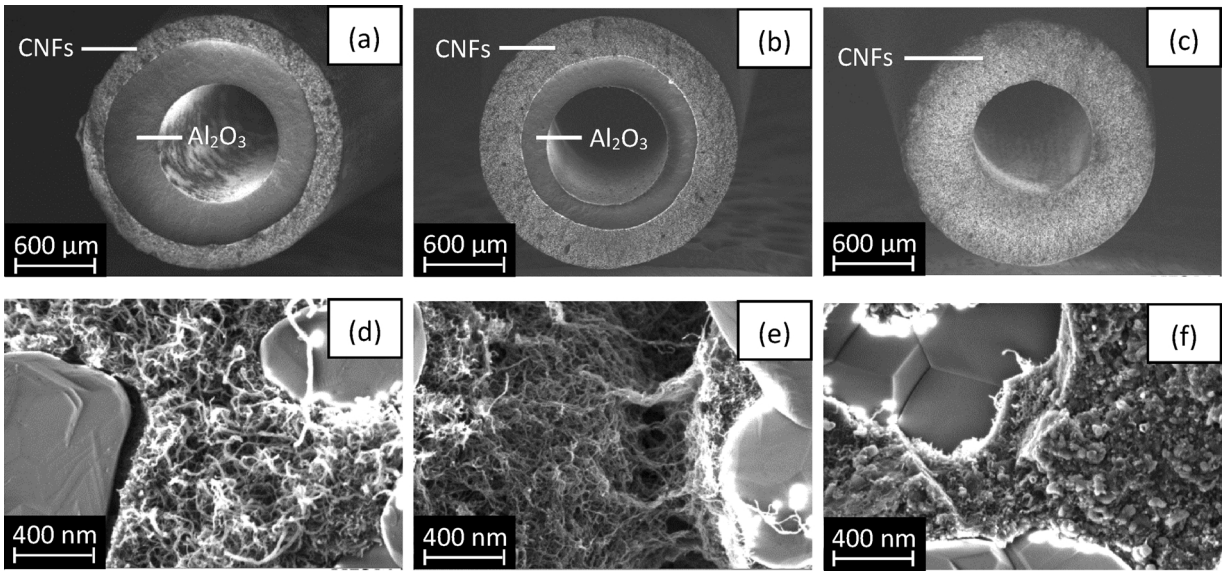

Fig. 2. HRSEM pictures of cross-sections of the three membrane reactors with different CNF growth times, a) 15 min, b) 22.5 min and c) 45 min. High magnification of the alumina macropores filled with CNFs are shown in d), e) and f) for the samples grown for 15, 22.5 and 45 min respectively.

The carbon content of the membrane reactor was determined with an analytic balance by weighing the reactor before and after CNF growth. The fraction of the pore volume filled with carbon was estimated based on the amount of CNFs and the void fraction of the α-Al_2O_3, measured with Hg porosimetry (Quantachrome Poremaster PM33). The palladium loading was determined for every membrane reactor using X-ray fluorescence spectroscopy, XRF (Philips PW 1480).

3. Results

3.1. Sample preparation

The appearance of the external surface of the samples prepared with different growth times (15, 22.5 and 45 min) is very similar, all presenting a fully and homogeneously covered surface. However, noticeable differences can be observed from the cross-sections. Fig. 2 shows the location of CNFs through the wall of the alumina fiber after different CNF growth times. After 45 min, the wall is filled with 8.0 wt% CNFs (Table 1) throughout the cross-section (Fig. 2c). In contrast, shorter growth time results in lower CNF coverage (down to 3.2 wt% for 15 min, Table 1), which is caused by preferential filling of the outer zone of the cross-section with CNFs. The thickness of the outer layer containing CNFs is presented in Table 1; note that the transition between the zones with and without CNFs is remarkably sharp (Fig. 2a and b, 3a). Fig. 2d–f shows that the apparent density at a fixed location of the CNFs increases with growth time.

Fig. 3a shows the interface between the regions with and without CNFs for the 22.5 min sample. Fig. 3b depicts the curly and entangled morphology of the CNFs, while Fig. 3c shows alumina grains in the region without CNFs. These alumina grains contain small nickel particles, confirming that the lack of CNFs is not caused by absence of nickel particles.

Table 1
Physical properties of the membrane reactors.

CNF thickness (µm)	200	320	500
CNF growth time (min)	15	22.5	45
Carbon percentage (wt.%)	3.2	5.5	8.0
Total CNF pore filling (vol%)	11	20	29
CNF pore filling in carbon region (vol%)	24	27	29
Surface area (m^2/g reactor)	6.5	10.1	22.0
Pd loading (g Pd/100 g reactor)	0.045	0.06	0.077
Pd particle size (nm)	8–9	8–9	8–9

Both the BET surface area and the amount of palladium scale with the amount of CNFs present in the alumina wall. Short CNF growth times result in a small amount of CNFs and therefore low surface area as well as low palladium loading. However, the differences in palladium loading are relatively less compared to CNF amount and surface area. The palladium particle size was very similar, typically 8–9 nm, in all the membrane reactors, based on HRSEM (not shown). Pd could be detected with EDX exclusively in the zone containing CNFs in Fig. 2b, despite the overall low Pd loading, whereas no Pd could be detected in the zone without any CNFs. Clearly, Pd is dominantly located within the confined CNF containing regions.

Two different values to determine pore filling are shown in Table 1. 'CNF pore filling in carbon region' takes into account exclusively the volume of the alumina pores that actually contain CNFs, while´total CNF pore filling' represents an averaged value considering the pore volume of the entire alumina tube.

3.2. Catalytic results

Fig. 4 shows that the selectivity of the ammonia by-product increases with increasing hydrogen concentration supplied through the PDMS membrane. The thinner the CNF region is, the higher the ammonia selectivity becomes. For example, the sample with a CNF thickness of 200 µm reaches 100% ammonia selectivity with high hydrogen concentrations (50–100%).

Fig. 5 shows that all three samples present different activities at a given hydrogen concentration. The activity of the samples with CNF thicknesses of 320 and 500 µm decreases when increasing hydrogen concentration. The sample with a CNF thickness of 200 µm presents the opposite behaviour.

The sample with a CNF thickness of 320 µm was also tested at a higher flow rate (0.15 ml/min). Although the conversion decreased down to 25%, the ammonia selectivity remained almost unchanged (from 45% to 41%).

Fig. 6 shows that the crushed sample with full CNF coverage (500 µm thickness) shows an increase in catalytic activity and ammonia selectivity when increasing hydrogen concentration. Remarkably, the surprising decrease in activity with hydrogen concentration (Fig. 5) changes to the opposite trend (Fig. 6) by crushing the membrane, which is much more usual.

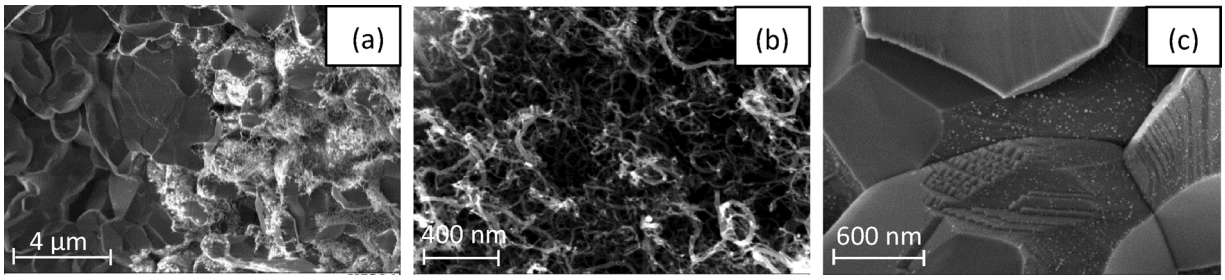

Fig. 3. Cross-sectional view of the sample with a CNF growth of 22.5 min, a) interface between CNFs and bare alumina, b) CNF morphology, c) bare alumina grains with nickel particles.

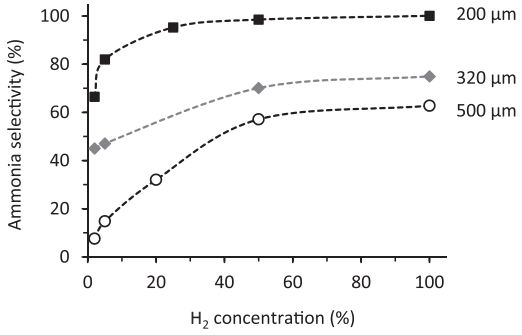

Fig. 4. Effect of hydrogen concentration on ammonia selectivity for the membrane reactors with different thickness of the layer filled with CNFs. Experiments were performed with 44 µmol/L nitrite solution with a liquid flow rate of 0.05 ml/min at room temperature.

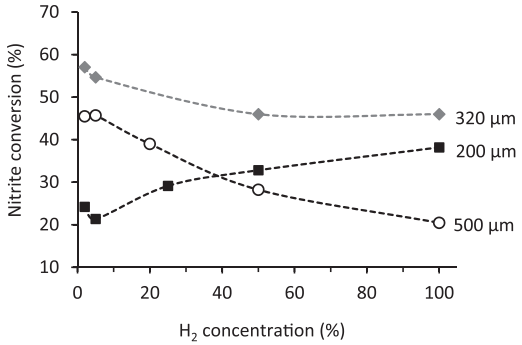

Fig. 5. Effect of hydrogen concentration on the nitrite conversion for the membrane reactors with different thickness of the layer filled with CNFs. Experiments were performed with 44 µmol/L nitrite solution with a liquid flow rate of 0.05 ml/min at room temperature.

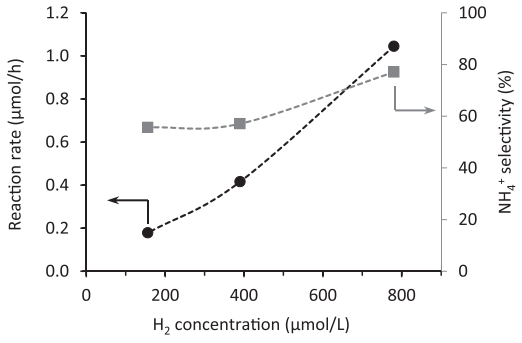

Fig. 6. Effect of hydrogen concentration on the reaction rate and the ammonia selectivity for the crushed reactor with full CNF coverage (45 min CNF growth). Tests were performed at room temperature with a nitrite solution of 217 µmol/L.

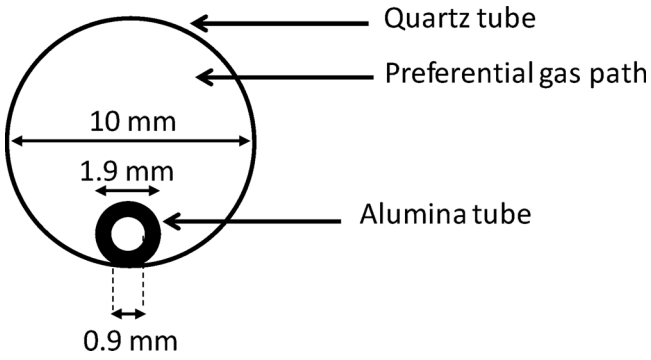

Fig. 7. Scheme of the alumina tube inside the quartz reactor during CNF growth. Note that dimensions are not proportional.

4. Discussion

4.1. Egg-shell catalyst induced by diffusion limitations

CNF growth initiates at the outer shell of the α-alumina tube. The zone with CNFs moves to the centre of the tube with increasing growth time, generating egg-shell structures. This is caused by a gas flow resistance inside the alumina tube due to the small diameter of the inner tube (0.9 mm, Fig. 7); the area of the cross-section of the reactor tube excluding the alumina tube is two orders of magnitude larger (76 mm^2) than the area inside the tube (0.64 mm^2).

Since the gas flow prefers the path with less resistance, the gas mainly flows outside of the alumina tube rather than inside. In other words, the gas inside the alumina tube will be nearly stagnant and the ethylene transport inside the tube will mainly occur *via* molecular diffusion. Therefore, CNFs will grow on the inside wall at both ends of the tube, but only for a typical distance of 2–3 mm due to ethylene exhaustion. The convective gas flow outside of the alumina tube provides reactive gas to the entire outer wall of the alumina. Ethylene and hydrogen diffusing through the outside surface of the alumina tube generate a CNF layer growing from the outside inwards the macropores in the alumina wall. It is well known that nickel particles deactivate during CNF synthesis [39]; Fig. 8 confirms the same for this study. Thus, after deactivation of the outer layer, ethylene penetrates deeper in the alumina wall, shifting the zone where CNFs form inwards. Nevertheless, CNFs become more densely packed at longer growth times (23% and 29% of pore volume filled in the CNF region after 15 and 45 min respectively, Table 1). Fig. 2d, e and f visually confirm that CNFs grown during 45 min appear denser, filling a larger fraction of the alumina macropores. However, the remaining pore volume is still significant (> 70%), enabling diffusion of ethylene and hydrogen to the deeper layer via the more densely filled outer layer.

The presence of nickel particles near the inner wall of the alumina tube (Fig. 3c) clearly confirms that the CNF distribution in the alumina tube after 15 and 22.5 min is not due to mal-distribution of nickel particles. Instead, diffusion limitation of ethylene inside the macropores in the wall of the alumina tube is likely responsible. This is further

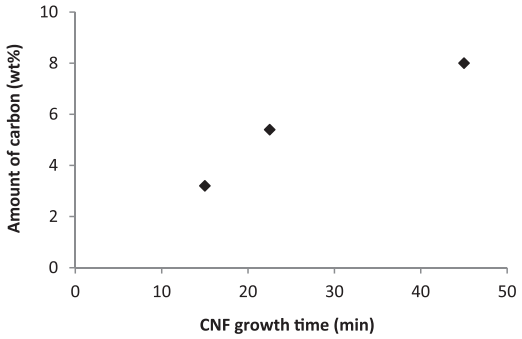

Fig. 8. Amount of carbon in the alumina tube when varying the CNF growth time.

supported by the observation that the alumina tube contains homogeneously distributed CNFs throughout the wall at both outer ends over a distance of typically 3 mm as discussed above. Notice that the outer ends of every sample were removed before catalytic testing.

4.2. Ammonia selectivity

The H/N ratio of reaction intermediates on the surface of the catalyst strongly influences selectivity to ammonia [32,35,40]. High H/N ratios lead to high ammonia selectivity while low ratios favour the formation of nitrogen. Clearly, the selectivity to ammonia increases with increasing hydrogen concentration (Fig. 4). In fact, ammonia formation requires three hydrogen molecules per nitrite (equation 4) while formation of nitrogen requires only one and a half (equation 3). Accordingly, low H coverage of the palladium catalyst is needed to suppress ammonia formation. Obviously, an optimum value exists, as too low H-surface coverage would induce very low rates.

$$2NO_2^- + 3H_2 + 2H^+ \xrightarrow{Pd} N_2 + 4H_2O \quad (3)$$

$$NO_2^- + 3H_2 + 2H^+ \rightarrow NH_4^+ + 2H_2O \quad (4)$$

Remarkably, all samples present very different selectivity, although all follow the same trend with hydrogen concentration (Fig. 4). Fig. 9 confirms that the selectivity to ammonia compared at constant conversion level increases in the order 500 μm < 320 μm < 200 μm, when the conversion is at least 30%. Therefore, the same trend observed in Fig. 4 is clearly not caused by differences in conversion level. The differences are attributed to different reactant concentration profiles through the wall of the membrane reactor.

Fig. 10 shows qualitatively the profiles of concentrations of hydrogen and nitrite inside the wall of the catalytic membrane reactor. As discussed above, the selectivity is controlled by the H/N ratio on the catalyst surface. This ratio varies strongly with the radial position (due to concentration gradients through the wall) as well as along the axial position, as conversion levels are well above differential conditions.

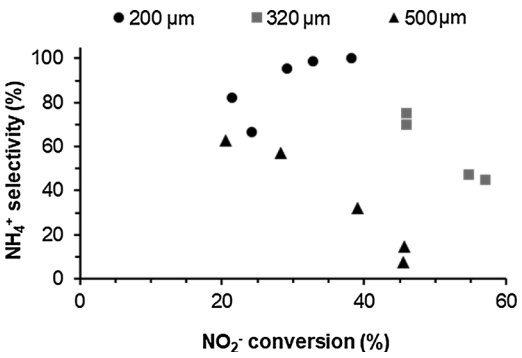

Fig. 9. Conversion selectivity plot for three membrane reactors with different thickness of the layer filled with CNFs. Experiments were performed with 44 μmol/L nitrite solution with a liquid flow rate of 0.05 ml/min at room temperature.

Fig. 10a shows that in case of a thin layer (200 μm) filled with CNFs containing Pd, nitrite concentration reaching the palladium active sites will be relatively low since the molecular flux through the macropores in the bare alumina zone is inversely proportional to the diffusion distance, *i.e.* the thickness of the bare alumina zone. Clearly, nitrite needs to diffuse through the alumina macropores filled with stagnant water before reaching the region with CNFs and active palladium particles. It was estimated that when operating at 2% hydrogen concentration, the nitrite concentration reaching the reaction zone will decrease by 80% (SI Appendix A). Additionally, the relatively low nitrite concentration will meet with a relatively high hydrogen concentration since the diffusion distance of hydrogen is short due to the proximity of the CNF layer to the PDMS membrane. Additionally, the PDMS membrane does not induce a significant hydrogen gradient because the membrane is very thin (10–15 μm) and the hydrogen permeability is large ($\sim 10^{-4}$ cm^2/s [41]); a concentration decrease in the order of only 1% was estimated (SI, Appendix A). As a result, a high hydrogen concentration is combined with a low nitrite concentration, leading to high H/N ratios and consequently high selectivity to ammonia.

In contrast, when Pd on the CNFs is located throughout the wall of the membrane reactor (Fig. 10c), nitrite concentration entering the reaction zone is significantly higher than for thin CNF layers. Additionally, the hydrogen flux will be affected by a larger reaction zone and therefore a lower averaged hydrogen concentration is expected. In this scenario, relatively low H/N ratios are expected causing low selectivity to ammonia (Fig. 4).

Fig. 10b (CNF thickness of 320 μm) depicts an intermediate situation between Fig. 10a and c. Nitrite concentration entering the reaction zone will be higher than in Fig. 10a but lower than in Fig. 10c. On the other hand, the average hydrogen concentration in the reaction zone will be higher than in Fig. 10c but lower than in Fig. 10a. This will lead to intermediate values of both the H/N as well as the ammonia selectivity (Fig. 4).

Ideally, to minimize the formation of ammonia, the active sites on the CNFs should be positioned closer to the inner wall rather than to the outer wall of the membrane reactor. However, this could not be achieved since CNFs start growing from the reactor shell. Future work will focus on the synthesis of a catalytic reactor that presents the active phase near the liquid stream. An option that is being explored is using a CNF layer at the outer surface (15 min of CNF growth) combined with a PDMS membrane at the inner surface. In this configuration, the liquid flow would be fed to the reactor shell and the hydrogen gas stream to the inner tube. Alternatively, a thicker PDMS membrane can be coated to further increase the resistance to hydrogen diffusion. Please note that we use the term 'synthesis' here for the catalytic reactor because it is in essence at the same time a shaped single catalyst particle.

4.3. Catalytic activity

The difference in activity for the three reactors with different Pd-distributions (Fig. 5) is also determined by the concentration gradients of the reactants inside the reaction zone. The reaction rate per mol palladium (Fig. 11) shows that the minor variations in palladium loading (Table 1) are not responsible for this difference in activity. It should be noted that the palladium particle size was also constant.

Surprisingly, hydrogen concentration shows quite different effects on catalyst activity in the three catalytic reactors. Figs. 5 and 10 show that the samples with CNF thickness of 320 and 500 μm are negatively affected by increasing hydrogen concentration, while the activity of the sample with a CNF thickness of 200 μm clearly benefits from an increase in hydrogen concentration, as would be expected. In other words, the apparent order in hydrogen is negative for the thicker CNF layers. This effect is clearly caused by the distribution of active sites in the membrane reactors and certainly not by the catalyst itself because a crushed reactor, operated as fixed bed, shows a positive apparent order

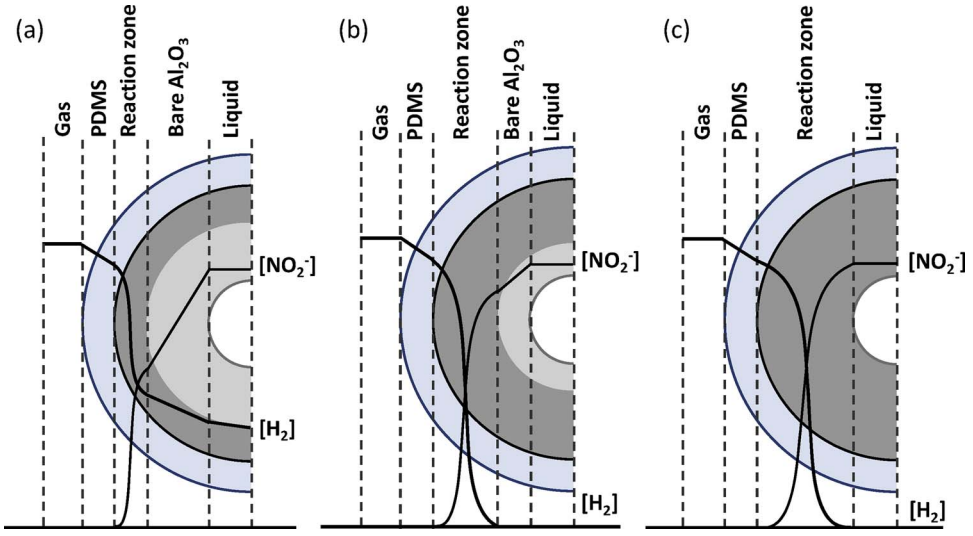

Fig. 10. Qualitative concentrations profiles for hydrogen and nitrite inside the wall of the membrane reactor for the three different distributions of the active phase by changing the thickness of the zone containing CNFs of a) 200 μm, b) 320 μm and c) 475 μm. The zones correspond to the gas phase, the PDMS membrane, the reaction zone, the bare alumina and the liquid phase in the central channel, all separated by doted lines.

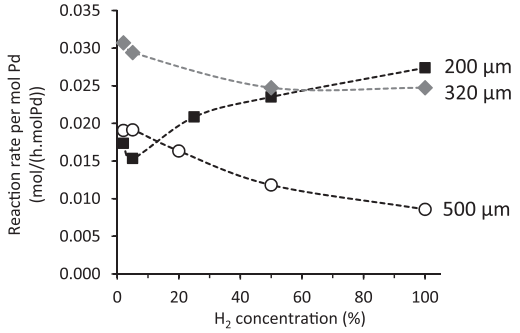

Fig. 11. Average reaction rate of nitrite per mol of palladium as a function of hydrogen concentration.

in hydrogen (Fig. 6), in agreement with literature [35,42,43].

The nitrite concentration in this study is similar to the lowest concentrations applied in the kinetic studies in literature, whereas the hydrogen concentrations are very similar. This would suggest that the kinetic descriptions in literature should also be valid for the conditions applied in this study, as temperature and pH are similar as well. However, kinetic experiment in conventional reactors have in common that concentration gradients in the catalyst particles, if any, can be qualitatively described as in Fig. 12a, quite different for the membrane reactor presented in Fig. 12b. Clearly, the ratio hydrogen/nitrite varies in a much wider window in a catalytic membrane reactors compared to in a catalyst particle, not only because the diffusion distance in the membrane is larger, but especially because the profiles are opposite instead of parallel in catalyst particles. In other words, in the catalytic membrane reactor, some of the palladium particles are exposed to extremely low hydrogen concentration in combination with usual nitrite concentration, as well as at the same time the opposite situation occurs at a different position in the catalytic membrane. Consequently, surface coverage of H and nitrite, or any stable N-intermediate surface compound on Pd [44,45] will strongly vary locally; much stronger than in fixed bed or slurry catalyst.

It is well known that, assuming a Langmuir-Hinshelwood mechanism [31], surface coverages influence experimental kinetic parameters including reaction orders and activation energies. The apparent order in e.g. hydrogen can become negative in the case of competitive adsorption with nitrite, when the H-surface-coverage would approach 100%. The observation that the reactors with a thick active zone exhibit a negative order in hydrogen, indicates that the performance of these reactors is importantly dominated by the zone in the active layer that is rich in hydrogen and poor in nitrite. In fact, the H/N ratio is apparently extremely high as competitive adsorption and negative order in hydrogen was never reported in studies using catalyst particles, with concentration gradients as in Fig. 12a. Mimicking the situation in the H-rich zone in the membrane reactor experimentally is apparently not possible as extremely low nitrite concentrations would be required.

Clearly, the catalytic reactor with a thin active zone exhibits usual kinetics, i.e. a positive order in hydrogen. This may indicate that the concentration gradients do not develop completely, preventing complete exhaustion of the reactants. In addition, the metal loading is lower (see Table 1), causing less developed concentration gradients. A full description of the performance of the membrane reactors would ask for modelling of both radial gradients, as discussed above, as well as axial gradients as the conversion levels are significant. This, however, would

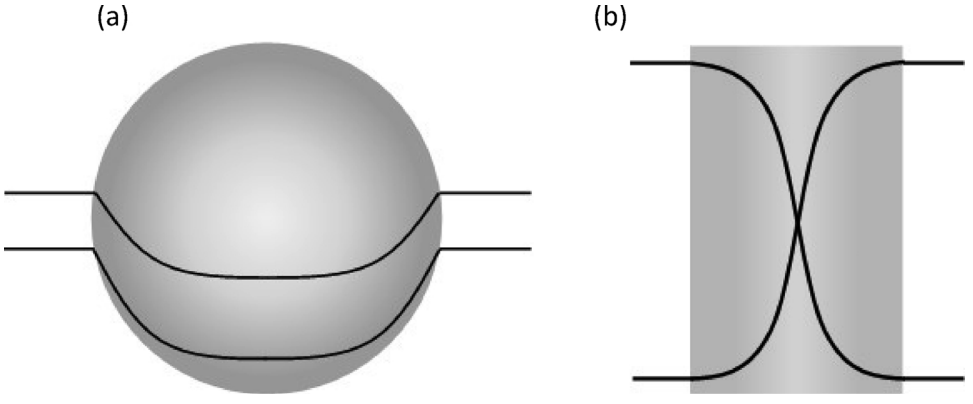

Fig. 12. Reactant profiles in a) catalyst particles, b) membrane reactors.

require a kinetic description for the full window of concentrations and concentration ratios, which is not available at this time.

Finally, catalytic membrane contactor reactors may be considered as a single catalyst particle, acting as reactor at the same time. However, variation of the distribution of active sites through the porous support influences the performance *via* concentration-gradients in a clearly different manor.

5. Conclusions

Three membrane reactors were fabricated with different well-controlled distributions of the active phase through the alumina wall. Eggshell distribution of CNFs was obtained due to diffusion limitation of ethylene during CNF growth; the thickness of the zone containing CNFs in the macro-pores of the alumina tube increases with time. As the nickel catalyst particles, responsible for CNF synthesis, deactivate slowly, the reaction front of CNF-growth slowly moves inside the tube of the alumina wall. The diffusion lengths of both nitrite and hydrogen during nitrite hydrogenation are determined by the CNF distribution because palladium is deposited on the CNFs. It was proven that, inducing different concentration gradients of nitrite and hydrogen, the activity and selectivity of nitrite hydrogenation can be manipulated, *i.e.* thicker reactive zones are more selective towards nitrogen. The thicker reactive zones cause local exhaustion of nitrite, resulting in a negative apparent order in hydrogen.

Acknowledgments

This work is supported by NanoNextNL, a micro and nanotechnology consortium of the Government of The Netherlands and 130 partners. We are thankful to K. Altena – Schildkamp and T.M.L Velthuizen for chemical analysis, and to M. Smithers for HRSEM measurements.

Appendix A. Supplementary data

Supplementary data associated with this article can be found, in the online version, at http://dx.doi.org/10.1016/j.apcatb.2017.10.058.

References

[1] H.C. Aran, H. Klooster, J.M. Jani, M. Wessling, L. Lefferts, R.G.H. Lammertink, Influence of geometrical and operational parameters on the performance of porous catalytic membrane reactors, Chem. Eng. J. 207–208 (2012) 814–821.
[2] G. Biardi, G. Baldi, Three-phase catalytic reactors, Catal. Today 52 (1999) 223–234.
[3] G. Chen, J. Yue, Q. Yuan, Gas-liquid microreaction technology: recent developments and future challenges, Chin. J. Chem. Eng. 16 (2008) 663–669.
[4] J.K. Chinthaginjala, Hairy Foam: Thin Layers of Carbon Nanofibers as Catalyst Support for Liquid Phase Reactions, In: CPM, University of Twente, Enschede, 2010, p. 149.
[5] J.A.M. Andrzej Cybulski, Structured Catalysts and Reactors, second ed., (2006) New York.
[6] M.P. Duduković, F. Larachi, P.L. Mills, Multiphase catalytic reactors: a perspective on current knowledge and future trends, Catal. Rev. – Sci. Eng. 44 (2002) 123–246.
[7] P.A. Ramachandran, R.V. Chaudhari, Three-phase Catalytic Reactors, Gordon and Breach Science Publishers, New York, 1983.
[8] C.N. Satterfield, Trickle-bed reactors, AIChE J. 21 (1975) 209–228.
[9] J. Gascon, J.R. van Ommen, J.A. Moulijn, F. Kapteijn, Structuring catalyst and reactor – an inviting avenue to process intensification, Catal. Sci. Technol. 5 (2015) 807–817.
[10] K. Pangarkar, T.J. Schildhauer, J.R. van Ommen, J. Nijenhuis, F. Kapteijn, J.A. Moulijn, Structured packings for multiphase catalytic reactors, Ind. Eng. Chem. Res. 47 (2008) 3720–3751.
[11] J. Gascon, J.R. van Ommen, J.A. Moulijn, F. Kapteijn, Structuring catalyst and reactor–an inviting avenue to process intensification, Catal. Sci. Technol. 5 (2015) 807–817.
[12] A. Cordier, E. Flahaut, C. Viazzi, C. Laurent, A. Peigney, In situ CCVD synthesis of carbon nanotubes within a commercial ceramic foam, J. Mater. Chem. 15 (2005) 4041.
[13] P.W.A.M. Wenmakers, J. van der Schaaf, B.F.M. Kuster, J.C. Schouten, Hairy Foam: carbon nanofibers grown on solid carbon foam. A fully accessible high surface area, graphitic catalyst support, J. Mater. Chem. 18 (2008) 2426–2436.
[14] N. Jarrah, J. Vanommen, L. Lefferts, Mechanistic aspects of the formation of carbon-nanofibers on the surface of Ni foam: a new microstructured catalyst support, J. Catal. 239 (2006) 460–469.
[15] J.K. Chinthaginjala, J.H. Bitter, L. Lefferts, Thin layer of carbon-nano-fibers (CNFs) as catalyst support for fast mass transfer in hydrogenation of nitrite, Appl. Catal. A Gen. 383 (2010) 24–32.
[16] M. Cantoro, V.B. Golovko, S. Hofmann, D.R. Williams, C. Ducati, J. Geng, B.O. Boskovic, B. Kleinsorge, D.A. Jefferson, A.C. Ferrari, B.F.G. Johnson, J. Robertson, Wet catalyst assisted growth of carbon nanofibers on complex three-dimensional substrates, Diamond Relat. Mater. 14 (2005) 733–738.
[17] Y. Matatov-Meytal, M. Sheintuch, Catalytic fibers and cloths, Appl. Catal. A Gen. 231 (2002) 1–16.
[18] H.C. Aran, Porous Ceramic and Metallic Microreactors, In: Sfi, University of Twente, Enschede, 2011, p. 126.
[19] A. Julbe, D. Farrusseng, C. Guizard, Porous ceramic membranes for catalytic reactors — overview and new ideas, J. Membr. Sci. 181 (2001) 3–20.
[20] R. Dittmeyer, K. Svajda, M. Reif, A review of catalytic membrane layers for Gas/Liquid reactions, Top. Catal. 29 (2004) 3–27.
[21] S. Mota, S. Miachon, J.C. Volta, J.A. Dalmon, Membrane reactor for selective oxidation of butane to maleic anhydride, Catal. Today 67 (2001) 169–176.
[22] M. Huuhtanen, P.K. Seelam, T. Kolli, E. Turpeinen, R.L. keiski, 11 – advances in catalysts for membrane reactors, in: A. Basile (Ed.), Handbook of Membrane Reactors, Woodhead Publishing, 2013, pp. 401–432.
[23] R. Dittmeyer, V. Höllein, K. Daub, Membrane reactors for hydrogenation and dehydrogenation processes based on supported palladium, J. Mol. Catal. A Chem. 173 (2001) 135–184.
[24] M. Huuhtanen, P.K. Seelam, T. Kolli, E. Turpeinen, R.L. Keiski, Advances in catalysts for membrane reactors (2013) 401–432.
[25] S. Miachon, J.-A. Dalmon, Catalysis in membrane reactors: what about the catalyst? Top. Catal. 29 (2004) 59–65.
[26] H.C. Aran, J.K. Chinthaginjala, R. Groote, T. Roelofs, L. Lefferts, M. Wessling, R.G.H. Lammertink, Porous ceramic mesoreactors: a new approach for gas-liquid contacting in multiphase microreaction technology, Chem. Eng. J. 169 (2011) 239–246.
[27] A. Pashkova, R. Dittmeyer, N. Kaltenborn, H. Richter, Experimental study of porous tubular catalytic membranes for direct synthesis of hydrogen peroxide, Chem. Eng. J. 165 (2010) 924–933.
[28] M. Vospernik, A. Pintar, G. Berčič, J. Batista, J. Levec, Potentials of ceramic membranes as catalytic three-phase reactors, Chem. Eng. Res. Des. 82 (2004) 659–666.
[29] H.C. Aran, S. Pacheco Benito, M.W.J. Luiten-Olieman, S. Er, M. Wessling, L. Lefferts, N.E. Benes, R.G.H. Lammertink, Carbon nanofibers in catalytic membrane microreactors, J. Membr. Sci. 381 (2011) 244–250.
[30] S. Horold, T. Tacke, K.D. Vorlop, Catalytical removal of nitrate and nitrite from drinking water: 1. Screening for hydrogenation catalysts and influence of reaction conditions on activity and selectivity, Environ. Technol. 14 (1993) 931–939.
[31] A. Pintar, G. Berčič, J. Levec, Catalytic liquid-phase nitrite reduction: kinetics and catalyst deactivation, AIChE J. 44 (1998) 2280–2292.
[32] C. Franch, R.G.H. Lammertink, L. Lefferts, Partially hydrophobized catalyst particles for aqueous nitrite hydrogenation, Appl. Catal. B Environ. 156-157 (2014) 166–172.
[33] D. Shuai, J.K. Choe, J.R. Shapley, C.J. Werth, Enhanced activity and selectivity of carbon nanofiber supported Pd catalysts for nitrite reduction, Environ. Sci. Technol. 46 (2012) 2847–2855.
[34] S.D. Ebbesen, B.L. Mojet, L. Lefferts, Effect of pH on the nitrite hydrogenation mechanism over pd/Al 2O3 and Pt/Al2O3: details obtained with ATR-IR spectroscopy, J. Phys. Chem. C 115 (2011) 1186–1194.
[35] J.K. Chinthaginjala, L. Lefferts, Support effect on selectivity of nitrite reduction in water, Appl. Catal. B Environ. 101 (2010) 144–149.
[36] K. Wada, T. Hirata, S. Hosokawa, S. Iwamoto, M. Inoue, Effect of supports on Pd-Cu bimetallic catalysts for nitrate and nitrite reduction in water, Catal. Today 185 (2012) 81–87.
[37] R. Brunet Espinosa, D. Rafieian, R.G.H. Lammertink, L. Lefferts, Carbon nano-fiber based membrane reactor for selective nitrite hydrogenation, Catal. Today 273 (2016) 50–61.
[38] S. Hörold, K.D. Vorlop, T. Tacke, M. Sell, Development of catalysts for a selective nitrate and nitrite removal from drinking water, Catal. Today 17 (1993) 21–30.
[39] M.L. Toebes, J.H. Bitter, A. Jos Van Dillen, K.P. De Jong, Impact of the structure and reactivity of nickel particles on the catalytic growth of carbon nanofibers, Catal. Today 76 (2002) 33–42.
[40] K. Wada, T. Hirata, S. Hosokawa, S. Iwamoto, M. Inoue, Effect of supports on Pd–Cu bimetallic catalysts for nitrate and nitrite reduction in water, Catal. Today 185 (2012) 81–87.
[41] M. Sadrzadeh, K. Shahidi, T. Mohammadi, Effect of operating parameters on pure and mixed gas permeation properties of a synthesized composite PDMS/PA membrane, J. Membr. Sci. 342 (2009) 327–340.
[42] I. Mikami, Y. Sakamoto, Y. Yoshinaga, T. Okuhara, Kinetic and adsorption studies on the hydrogenation of nitrate and nitrite in water using Pd-Cu on active carbon support, Appl. Catal. B Environ. 44 (2003) 79–86.
[43] Y. Matatov-Meytal, Cloth catalysts in water denitrification III. pH inhibition of nitrite hydrogenation over Pd/ACC, Appl. Catal. B Environ. 45 (2003) 127–134.
[44] S.D. Ebbesen, B.L. Mojet, L. Lefferts, Effect of pH on the nitrite hydrogenation mechanism over Pd/Al2O3 and Pt/Al2O3: details obtained with ATR-IR spectroscopy, J. Phys. Chem. C 115 (2011) 1186–1194.
[45] Y. Zhao, Colloidal Nanoparticles as Catalyst and Catalyst Precursors for Nitrite Hydrogenation, In: Cpm, University of Twente, Enschede, 2015, p. 133.